UNIVERSITÀ DI PARMA
ARCHIVIO DELLA RICERCA

University of Parma Research Repository

Cucurbit[7]uril-Dimethyllysine Recognition in a Model Protein

This is the peer reviewd version of the followng article:

Original
Cucurbit[7]uril-Dimethyllysine Recognition in a Model Protein / Guagnini, Francesca; Antonik, Paweł M.; Rennie, Martin L.; O'Byrne, Peter; Khan, Amir R.; Pinalli, Roberta; Dalcanale, Enrico; Crowley, Peter B.. - In: ANGEWANDTE CHEMIE. INTERNATIONAL EDITION. - ISSN 1433-7851. - 57:24(2018), pp. 7126-7130. [10.1002/anie.201803232]

Availability:
This version is available at: 11381/2847713 since: 2021-10-02T18:14:17Z

Publisher:
Wiley-VCH Verlag

Published
DOI:10.1002/anie.201803232

Terms of use:

Anyone can freely access the full text of works made available as "Open Access". Works made available

Publisher copyright

note finali coverpage

(Article begins on next page)

19 July 2025

Cucurbit[7]uril–Dimethyllysine Recognition in a Model Protein

Francesca Guagnini,[a][b] Paweł M. Antonik,[a] Martin L. Rennie,[a] Peter O'Byrne,[c] Amir R. Khan,[c] Roberta Pinalli,[b] Enrico Dalcanale,[b] and Peter B. Crowley*[a]

Abstract: Here, we provide the first structural characterization of host-guest complexation between cucurbit[7]uril (**Q7**) and dimethyllysine (KMe_2) in a model protein. Binding was dominated by complete encapsulation of the dimethylammonium functional group. While selectivity for the most sterically accessible dimethyllysine was observed both in solution and in the solid state, three different modes of **Q7**–KMe_2 complexation were revealed by X-ray crystallography. The crystal structures revealed also entrapped water molecules that persisted in solvating the ammonium group within the **Q7** cavity. Remarkable **Q7**–protein assemblies, including inter-locked octahedral cages that comprise 24 protein trimers, occurred in the solid state. Cucurbituril clusters appear to be responsible for these assemblies, suggesting a strategy to generate controlled protein architectures.

Over the past fifteen years the donut-shaped cucurbit[n]uril (**Qn**) has emerged as a versatile macrocyclic host for biomolecular recognition[1,2] with broad applications in protein sensing and regulation.[3-8] Tight, selective binding to N-terminal aromatic residues[3,4,7] has paved the way for the development of **Q8**-mediated dimerization,[9] polymerization[10] as well as ternary complex formation.[11] These advances are part of the growing field of supramolecular chemistry with proteins.[12-14] A wealth of structural evidence is available for protein recognition, and in some cases assembly, by supramolecular receptors.[4,11,14-21]

Cucurbiturils are attractive hosts for protein recognition due to their selective complexation in aqueous solution, driven by the release of high energy water from the hydrophobic cavity.[3,4,22-25] For example, **Q7** binds to the N-terminal phenylalanine of insulin with μM affinity in a complex that includes burial of the aromatic ring within the **Q7** cavity and ion-dipole interactions between the N-terminal ammonium and the carbonyl rim of **Q7**.[4] The larger **Q8** can accommodate the side chains of two aromatic residues.[3] While this binding mode has featured prominently in numerous **Qn**-protein systems,[9-11] **Qn** can interact also with lysine, in particular, methylated lysine side chains.[23,26-31] Mono-, di- and tri-methylation of the lysine ammonium (N^{ζ}) are common post translational modifications that occur most notably in histones, with vast ramifications for gene expression.[32] Methylated lysines (KMe_n) present unique hotspots for recognition by reader proteins that possess an aromatic cage motif. Consequently, synthetic receptors that recognize KMe_n hold great potential as probes to study biological systems and as inhibitors of protein-protein interactions.[32-38] **Q7**-KMe_n interactions have been characterized for the amino acids, reveal that the affinity increases dramatically with the degree of methylation.[28] Recent experiments with a KMe_3-containing histone peptide indicate a ~10-fold drop in K_d relative to the amino acid,[31] pointing to a favourable contribution by the N^{α} group[32]. To date, there are no literature reports of **Qn**-KMe_n binding with a protein. To address this gap we characterized the interactions of **Q7** with a protein that contains dimethyllysine (KMe_2) and thereby provide a stepping stone to new applications of **Q7** in protein interactions.

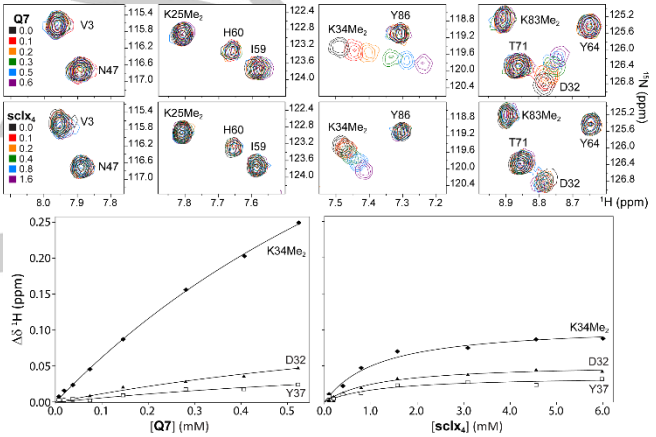

Figure 1. Upper panels. Spectral regions from overlaid ^{1}H-^{15}N HSQC spectra of RSL.KMe_2 in the presence of 0-0.6 mM **Q7** or 0-1.6 mM **sclx4**. Each panel provides data on at least one of the four potential binding sites. Resonance V3 is a reporter for $S1Me_2$ (the N-terminus). Significant chemical shift perturbations were observed for $K34Me_2$ and the resonances of adjacent residues only. **Lower panels.** NMR-derived binding curves for complex formation between RSL.KMe_2 and **Q7** or **sclx4**.

Although the affinity of **Q7**-KMe_n complexation increases with the degree of methylation[28] we studied KMe_2 as this modification is readily accessible in a model protein. *Ralstonia solanacearum* lectin (RSL), an extensively characterized and highly stable ~29 kDa trimer with a six-bladed β-propeller topology, was chosen as the model.[39-42] The protein was chemically dimethylated[31,41] to yield RSL.KMe_2 with four modified sites, $K25Me_2$, $K34Me_2$, $K83Me_2$ and the N-terminus $S1Me_2$. Complex formation with **Q7** was investigated by ^{1}H-^{15}N HSQC-monitored titrations in 20 mM potassium phosphate, 50 mM NaCl, pH 6.0 (Figure 1). The ^{1}H-^{15}N resonances were assigned by comparison to native RSL (Figure S1). A 3.8 mM **Q7** stock solution (SI methods[44]) was titrated against RSL.KMe_2 and resulted in reproducible, large upfield perturbations of the $K34Me_2$ amide resonance (Figure 1). The resonances of neighbouring residues W31, D32 and Y37 were affected also. No chemical shift changes occurred at the other possible binding sites ($S1Me_2$, $K25Me_2$ or $K83Me_2$) indicating selectivity for $K34Me_2$. Control experiments with native RSL

[a] F. Guagnini, Dr. P. M. Antonik, Dr. M. L. Rennie, Prof. Dr. P. B. Crowley
School of Chemistry, National University of Ireland Galway
University Road, Galway (Ireland)
E-mail: peter.crowley@nuigalway.ie
[b] F. Guagnini, Dr. R. Pinalli, Prof. Dr. E. Dalcanale
Dipartimento di Scienze Chimiche della Vita e della Sostenibilità Ambientale, Università di Parma and INSTM UdR Parma
Parco Area delle Scienze 17/A, 43124 Parma (Italy)
[c] P. O'Byrne, Dr. A. R. Khan
School of Biochemistry and Immunology, Trinity College Dublin, Dublin 2 (Ireland)
Supporting information for this article is given via a link at the end of the document.

indicated that there was no binding to **Q7** under these conditions (Figure S2). An analysis of Δδ as a function of the ligand concentration yielded shallow binding curves that fit to a K_d of ~1 mM (Figure 1 and SI methods). The limited solubility of **Q7** precluded saturation conditions in the NMR experiments. Attempts to obtain thermodynamic information by isothermal titration calorimetry (ITC) were thwarted by the lack of binding heats. Standard titrations of **Q7** into RSL.KMe_2 did not yield usable data. A reverse titration of 5.4 mM RSL.KMe_2 into 0.1 mM **Q7** also gave negligible heat changes (Figure S3). For comparison, NMR titrations were performed with the highly water soluble sulfonatocalix[4]arene (**sclx$_4$**). Similar to **Q7**,[28] this anionic receptor binds KMe_n with an affinity that increases with the degree of methylation.[45] Interestingly, **sclx$_4$** also bound selectively to K34Me_2 with a K_d of ~1 mM (Figure 1). Minor perturbations at V3 and K83Me_2 indicated that higher concentrations of **sclx$_4$** may result in binding at these sites.

Table 1. Crystal structures of RSL.KMe_2 in **Q7**-bound and -free forms.

Space Group / **PDB**	Res[a] (Å)	Precipitant and Buffer	[Q7] / [protein] (mM)[b]	Notes
*C*222$_1$ **6F7W**	1.3	20 % PEG 3350 0.2 M Na^+Malonate pH 7.0	2.3 / 1.0	Symmetric **Q7** No MeFuc
*F*432 **6F7X**	2.4	25 % PEG 3350 0.1 M Bis-Tris pH 5.5	1.1 / 1.5	Asymmetric **Q7** MeFuc bound
*P*63 **6F7Y**	1.6	20 % PEG 3350 0.2 M K^+Formate pH 7.3	2.3 / 1.5	No **Q7** bound No MeFuc

[a] See Table S1 for processing and refinement statistics.
[b] Initial concentrations in the crystallization drop.

Further insights into **Q7**-KMe_2 host-guest complexation were obtained by X-ray crystallography. Crystallization was achieved by using a sparse matrix screen (Jena JCSG++). Simple solutions containing ~20 % PEG and a buffer (over the pH range 5 - 8) were sufficient to prompt crystal growth. Cubic crystals were obtained when methyl-α-L-fucoside (MeFuc), a ligand to RSL, was included[46]. Rod shaped crystals also grew in the presence or absence of **Q7** (Figure S4). X-ray data collection was performed both in-house (Rigaku) and at the APS synchrotron (Argonne National Laboratory). The structures were solved by molecular replacement (SI methods, Table S1) and the presence of **Q7** was clear in the electron density maps (Figure S5). The rod shaped crystals proved to be devoid of **Q7**. Two crystal structures of RSL.KMe_2 in the **Q7**-bound and one structure in the **Q7**-free state are reported (Table 1). The latter structure provided useful details on the binding site in the absence of **Q7**.

The **Q7**-bound structures crystallized in the *C*222$_1$ or *F*432 space groups, with an asymmetric unit that comprised one RSL.KMe_2 trimer and three or two **Q7** ligands, respectively. Of the four potential binding sites, **Q7** complexation occurred exclusively at K34Me_2, consistent with the NMR observations (Figure 1). The high selectivity of **Q7** for K34Me_2 can be rationalized in terms of side chain accessibility[33]. The accessible surface area of the KMe_2 side chains (calculated as an average from all chains in the three crystal structures) was 160, 240 and 190 Å^2 for K25Me_2, K34Me_2 and K83Me_2, respectively. K34Me_2 was the most exposed side chain due to its location in a loop (residues 31-37), while K25Me_2 and K83Me_2 are in β-strands. Furthermore, K34Me_2 is flanked by G33 and G35 which confer steric accessibility and backbone mobility. Interestingly, three different modes of **Q7**-K34Me_2 binding were observed. In the *C*222$_1$ structure, ~220 Å^2 of K34Me_2 was buried in the cavity with both methyl substituents sitting in the central plane of **Q7**. In this orientation the Lys C^{γ}-C^{δ} bond was intersected by the plane of the rim carbonyl oxygens (Figure 2A). While all three K34Me_2 sites in the RSL.KMe_2 trimer were similar the data at 1.3 Å resolution permitted model building with alternate conformations of K34Me_2 in chains B and C (Figure S6). These conformations suggest that the side chain retained some mobility inside **Q7** and that the cavity was incompletely filled by KMe_2. This packing deficiency may contribute to the lower affinity of **Q7**-KMe_2 with respect to **Q7**-KMe_3.[28]

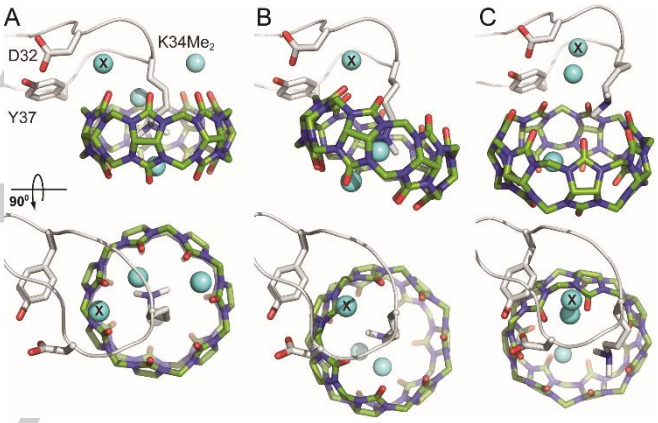

Figure 2. X-ray crystallography reveals complexation of **Q7** at K34Me_2 in RSL.KMe_2. The binding mode of **Q7** was significantly different in space groups (A) *C*222$_1$ and (B) *F*432. (C) The distal interaction at K34Me_2 in chain B of *F*432. Only the loop residues 31-37 are shown and oriented identically in each structure. Side chains D32, K34Me_2 and Y37 are represented as sticks. Residues 33 and 35 are Gly. Cyan spheres are water molecules and X denotes the conserved water (See Figure S7 for hydrogen bonding pattern). The upper and lower panels are related by a 90° rotation.

The *F*432 structure grew from conditions that contained a lower **Q7**:protein ratio compared to *C*222$_1$ (Table 1) and ligand binding was asymmetric with respect to the RSL.KMe_2 trimer. At chain A, **Q7** bound K34Me_2 (Figure 2B) in a fashion similar to that in the *C*222$_1$ structure. However, less of the side chain (~190 Å^2) was buried and the plane of the **Q7** rim carbonyl oxygens intersected the Lys C^{δ}-C^{ε} bond. At chain B, K34Me_2 formed a distal interaction (~130 Å^2 buried surface) with **Q7** (Figure 2C). This binding mode involved ion-dipole bonds between the ammonium group and two rim carbonyl oxygens ($N^{\zeta}\cdots$O=C ~3.0 Å). The opposite carbonyl portal formed a similar distal interaction with S1Me_2 of a symmetry related molecule. At chain C, the K34Me_2 was devoid of ligand and the electron density for this side chain was poor, indicative of disorder.

The complete burial of the cationic dimethylammonium group in the hydrophobic cavity of **Q7** raises interesting questions regarding solvation.[33] Indeed, two water molecules were refined together with the K34Me$_2$ side chain in the **Q7** cavity (Figure 2). In the *C*222$_1$ structure, one water formed a hydrogen bond with the K34Me$_2$ ammonium group ($O^W\cdots N^\zeta$ ~2.7 Å), while simultaneously hydrogen bonded to two rim carbonyl oxygens ($O^W\cdots O$=C <2.5 Å, Figure S7A). The second water was ~3.4 Å from the closest methyl substituent of the dimethylammonium group, and hydrogen bonded to a lower rim carbonyl, suggesting that the positive charge is partially dissipated to the electronegative rim. Similar interactions were observed in the *F*432 structure although in this case the water bonded to N^ζ was fully buried and did not interact with the rim carbonyls (Figure 2B). These observations are further intriguing since the cavity of **Q7** can accommodate eight water molecules, the release of which provides the driving force for guest binding.[2,22,24] This interpretation is based on studies of organic ammonium ions, with encapsulation of the hydrophobic portion inside **Q7** and ion-dipole interactions between the ammonium ion(s) and the rim carbonyls. In the case of KMe$_2$ encapsulation by **Q7**, six of the waters were displaced and two remaining waters solvated the tertiary ammonium ion inside the cavity (Figure 2).

Water also played a role in mediating **Q7** binding to the protein surface. A conserved water molecule (denoted X, Figures 2 and S7) was refined in each type of binding site and was present also in the **Q7**-free structure. In the *C*222$_1$ structure, water X was within hydrogen bond distance of three amide NH groups (D32, K34Me$_2$ and G35), the carbonyl of G35 and two **Q7** rim carbonyls (Figure S7). In the *F*432 structure, water X could hydrogen bond with three amides (D32, G33 and K34Me$_2$) and one **Q7** rim carbonyl. Interestingly, the loop 31-37 had a slightly different conformation at this site such that the amide NH of G35 was flipped out and pointed towards a rim carbonyl to form a unique protein-**Q7** hydrogen bond ($N^\alpha\cdots O$=C ~3.45 Å

Despite the high molecular weight (~1.2 kDa) and large surface area (~980 Å^2) of **Q7** only 3 or 4 residues on the protein surface were involved directly in ligand complexation. In addition to K34Me$_2$, neighbouring residues D32, Y37 were the only side chains to form van der Waals contacts with **Q7**. Notably, these two side chains are linked by a hydrogen bond ($O^\eta\cdots O^\delta$ ~2.6 Å) and retained similar positions in all of the binding sites even though the loop, K34Me$_2$ and **Q7** adopted different conformations (Figures 2 and S7). Apparently, the interaction of **Q7** and the phenol of Y37 were less important than other packing interactions.

Striking examples of protein architectures were observed in the crystal packing. The *C*222$_1$ and *F*432 structures involved trimeric and tetrameric clusters of **Q7**, respectively, suggesting the potential to use the **Q7**-KMe$_2$ complex as a pivot point for protein assembly (Figures 3 and 4).

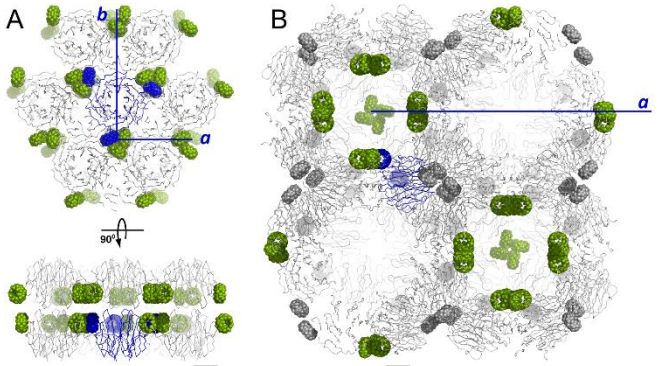

Figure 3. Crystal packing in space groups (A) *C*222$_1$ and (B) *F*432. Note the sheet assembly in *C*222$_1$ with **Q7** trimers mediating the packing. In *F*432 two interlocked cage assemblies were mediated via **Q7** tetramers (green). The distal binding **Q7** (see Figure 2C) is grey. Protein and ligand are shown as ribbons and spheres, respectively. The asymmetric unit and the unit cell axes are indicated in blue. Note that axis *a* is (A) ~50 or (B) ~200 Å.

Qn clusters are well-established in the literature, involving at least one CH$\cdots$O=C bond between pairs of macrocycles,[47-49] and a supramolecular triangle was reported recently for **Q8**.[48] In *C*222$_1$ (Figure 3A), sheets of trigonally-arrayed RSL.KMe$_2$ trimers are arranged around **Q7** trimers (Figure 4A). In addition to six CH$\cdots$O=C interactions, each **Q7** acted as a bidentate ligand to a central sodium ion. The cation was complexed by ion-dipole bonds from two of the rim carbonyls ($Na^+\cdots O$=C ~2.5 Å) resulting in an octahedral coordination geometry. Salts of alkali metals can increase **Qn** solubility through coordination of the rim carbonyls.[2,50] It is tempting to conclude that sodium was critical to the growth of the *C*222$_1$ crystal considering that **Q7**-free crystals grew from similar conditions in which sodium malonate was replaced by potassium formate (Table 1).

*F*432 is a rare space group characteristic of protein cages such as ferritin.[51] Remarkably, **Q7** at chain A mediated four-fold symmetric junctions to form a porous assembly of interlocked cages with 24 RSL.KMe$_2$ trimers disposed at the vertices of a regular octahedron (Figures 3B and 4B). This cage-like assembly has an internal diameter of ~6 nm, comparable to that of ferritin.[51] In addition to the lower **Q7**:protein ratio, the crystallization pH was also lower (relative to *C*222$_1$, Table 1) and may have favoured cage formation as the net charge on the protein switched from anionic to cationic (RSL p*I* ~6.8). Interestingly, the **Q7**-**Q7** interfaces (Figure 4) buried ~300 and ~240 Å^2 of surface (per **Q7**) in the *C*222$_1$ and *F*432 structures, while **Q7**-protein contacts buried ~240 Å^2 of the ligand surface. It can be assumed that the relatively low water solubility of **Q7** is conducive to the formation of **Q7**-mediated protein architectures. Furthermore, the **Q7** clusters at protein-protein interfaces may be an extension on the theme of macrocyclic molecular glues for protein assembly and crystallization[19-21].

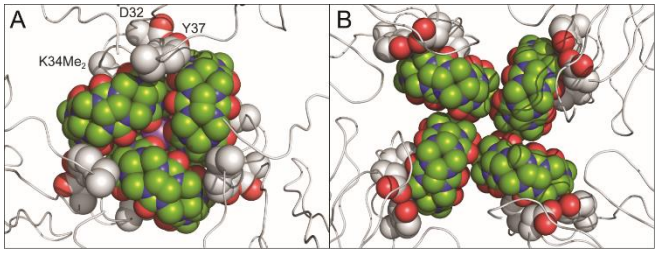

Figure 4. Trimeric and tetrameric cucurbituril clusters in space groups (A) $C222_1$ and (B) $F432$ in which **Q7**-**Q7** packing buried ~300 or ~240 Å^2 of ligand surface, respectively. In $C222_1$ the trimeric **Q7** formed an octahedral complex with a sodium cation (central, purple sphere). Side chains D32, K34Me$_2$ and Y37 are represented as spheres.

Supramolecular building blocks are increasingly popular as receptors for protein binding and assembly.[12-14] Examples include protein oligomerization mediated by calixarenes[15,16] and foldamers.[17] Anionic calixarenes have proven particularly useful for the assembly of cationic proteins.[16,19,21] The binding of **Qn** to N-terminal aromatic residues is an established route to controlled protein interactions.[4,9-11] Programmable assembly of dimers[9] and polymers[10] can be achieved *via* the combination of **Q8** with proteins that bear an N-terminal phenylalanine. This repertoire has been expanded now to include **Q7**-KMe$_2$ complexation and assembly. Contrary to amino acid[28] and peptide studies[31] we observed a modest affinity for the **Q7**-KMe$_2$ interaction in the model protein RSL.KMe$_2$ (Figure 1). Nevertheless, the affinity was sufficient to effect protein assembly in the solid state, with **Q7**-**Q7** packing playing pivotal roles (Figures 3 and 4). The poor water solubility of **Q7** is apparently advantageous in this regard. The pronounced selectivity of **Q7** for the most exposed KMe$_2$ (Figures 1 and 2) points to a simple strategy of engineered protein assemblies based on **Q7**-KMe$_2$ complexation. Finally, the tighter **Q7**-KMe$_3$ interaction[28] suggests that this motif can be employed to greater advantage than **Q7**-KMe$_2$ in protein assembly.

Acknowledgements

This research was supported by NUI Galway and Science Foundation Ireland (grants 13/ERC/B2912 and 13/CDA/2168 to PBC) and by University of Parma intramural funding (PhD fellowship to FG). B. Harhen and R. Doohan are thanked for assistance with mass spectrometry and NMR spectroscopy, respectively. We acknowledge the staff of NE-CAT at the Advanced Photon Source for assistance with data collection.

Keywords: cucurbituril • desolvation • macrocycle • molecular recognition • supramolecular chemistry

[1] J. W. Lee, S. Samal, N. Selvapalam, H. J. Kim, K. Kim, *Acc. Chem. Res.* **2003**, *36*, 621-630.

[2] S. J. Barrow, S. Kasera, M. J. Rowland, J. del Barrio, O. A. Scherman, *Chem. Rev.* **2015**, *115*, 12320-12406.

[3] L. M. Heitmann, A. B. Taylor, P. J. Hart, A. R. Urbach, *J. Am. Chem. Soc.* **2006**, *128*, 12574-12581.

[4] J. M. Chinai, A. B. Taylor, L. M. Ryno, N. D. Hargreaves, C. A. Morris, P. J. Hart, A. R. Urbach, *J. Am. Chem. Soc.* **2011**, *133*, 8810-8813.

[5] J. W. Lee, M. H. Shin, W. Mobley, A. R. Urbach, H. I. Kim, *J. Am. Chem. Soc.* **2015**, *137*, 15322-15329.

[6] S. Sonzini, A. Marcozzi, R. J. Gubeli, C. F. van der Walle, P. Ravn, A. Herrmann, O. A. Scherman, *Angew. Chem. Int. Ed.* **2016**, *55*, 14000-14004.

[7] W. Li, A. T. Bockus, B. Vinciguerra, L. Isaacs, A.R. Urbach, *Chem. Commun.* **2016**, *52*, 8537-8540.

[8] J. Murray, J. Sim, K. Oh, G. Sung, A. Lee, A. Shrinidhi, A. Thirunarayanan, D. Shetty, K. Kim, *Angew. Chem. Int. Ed.* **2017**, *56*, 2395-2398.

[9] H. D. Nguyen, D. T. Dang, J. L. van Dongen, L. Brunsveld, *Angew. Chem. Int. Ed*. **2010**, *49*, 895-898.

[10] C. Hou, J. Li, L. Zhao, W. Zhang, Q. Luo, Z. Dong, J. Xu, J. Liu, *Angew. Chem. Int. Ed.* **2013**, *52*, 5590-5593.

[11] P. J. de Vink, J. M.Briels, T. Schrader, L. G. Milroy, L. Brunsveld, C. Ottmann, *Angew. Chem. Int. Ed.* **2017**, *56*, 8998-9002.

[12] F. G. Klärner, T. Schrader, *Acc. Chem. Res.* **2013**, *46*, 967-978.

[13] Q. Luo, C. Hou, Y. Bai, R. Wang, J. Liu, *Chem. Rev.* **2016**, *116*, 13571-13632.

[14] S. van Dun, C. Ottmann, L.G. Milroy, L. Brunsveld, *J. Am. Chem. Soc.* **2017**, *139*, 13960-13968.

[15] R. E. McGovern, H. Fernandes, A. R. Khan, N. P. Power, P. B. Crowley, *Nat. Chem.* **2012**, *4*, 527-533.

[16] R. E. McGovern, A. A. McCarthy, P. B. Crowley, *Chem. Commun.* **2014**, *50*, 10412-10415.

[17] J. Buratto, C. Colombo, M. Stupfel, S. J. Dawson, C. Dolain, B. Langlois d'Estaintot, L. Fischer, T. Granier, M. Laguerre, B. Gallois, I. Huc, *Angew. Chem. Int. Ed.* **2014**, *53*, 883-887.

[18] D. Bier, S. Mittal, K. Bravo-Rodriguez, A. Sowislok, X. Guillory, J. Briels, C. Heid, M. Bartel, B. Wettig, L. Brunsveld, E. Sanchez-Garcia, T. Schrader, C. Ottmann, *J. Am. Chem. Soc.* **2017**, *139*, 16256-16263.

[19] M. L. Rennie, A. M. Doolan, C. L. Raston, P. B. Crowley, *Angew. Chem. Int. Ed.* **2017**, *56*, 5517-5521.

[20] A. M. Doolan, M. L. Rennie, P. B. Crowley, *Chem. Eur. J.* **2018**, *24*, 984-991.

[21] J. M. Alex, M. L. Rennie, S. Volpi, F. Sansone, A. Casnati, P. B. Crowley *Cryst. Growth Des.* **2018**, *18*, 2467–2473.

[22] F. Biedermann, V. D. Uzunova, O. A. Scherman. W. M. Nau, A. De Simone, *J. Am. Chem. Soc.* **2012**, *134*, 15318-15323.

[23] Y. Wang, J. R. King, P. Wu, D. L. Pelzman, D. N. Beratan, E. J. Toone, *J. Am. Chem. Soc.* **2013**, *135*, 6084-6091.

[24] F. Biedermann, W. M. Nau, H. J. Schneider, *Angew. Chem. Int. Ed.* **2014**, *53*, 11158-11171.

[25] D. Sigwalt, M. Šekutor, L. Cao, P. Y. Zavalij, J. Hostaš, H. Ajani, P. Hobza, K. Mlinarić-Majerski, R. Glaser, L. Isaacs, *J. Am. Chem. Soc.* **2017**, *139*, 3249-3258.

[26] D. M. Bailey, A. Hennig, V. D. Uzunova, W. M. Nau, *Chem. Eur. J.* **2008**, *14*, 6069-6077.

[27] H. Zhang, M. Grabenauer, M. T. Bowers, D. V. Dearden, *J. Phys. Chem. A* **2009**, *113*, 1508-1517.

[28] M. A. Gamal-Eldin, D. H. Macartney, *Org. Biomol. Chem.* **2013**, *11*, 488-495.

MANUSCRIPT

[29] J. W. Lee, H. H. Lee, Y. H. Ko, K. Kim, H. I. Kim, *J. Phys. Chem B.* **2015**, *119*, 4628-4636.

[30] E. Kovalenko, M. Vilaseca, M. Díaz-Lobo, A. N. Masliy, C. Vicent, V. P. Fedin, *J. Am. Soc. Mass Spectrom.* **2016**, *27*, 265-276.

[31] J. Lee, L. Perez, Y. Liu, H. Wang, R. J. Hooley, W. Zhong, *Anal. Chem.* **2018**, *90*, 1881-1888.

[32] J. E. Beaver, M. L. Waters, *ACS Chem. Biol.* **2016**, *11*, 643-653.

[33] R. E. McGovern, B. D. Snarr, J. A. Lyons, J. McFarlane, A. L. Whiting, I. Paci, F. Hof, P. B. Crowley, *Chem. Sci.* **2015**, *6*, 442-449.

[34] H. Peacock, C. C. Thinnes, A. Kawamura, A. D. Hamilton, *Supramol. Chem.* **2016**, 28, 575-581.

[35] R. Pinalli, G. Brancatelli, A. Pedrini, D. Menozzi, D. Hernández, P. Ballester, S. Geremia, E. Dalcanale, *J. Am. Chem. Soc.* **2016**, *138*, 8569-8580.

[36] I. N. Gober, M. L. Waters, *J. Am. Chem. Soc.* **2016**, *138*, 9452-9459.

[37] Y. Liu, L. Perez, A. D. Gill, M. Mettry, L. Li, Y. Wang, R. J. Hooley, W. Zhong, *J. Am. Chem. Soc.* **2017**, *139*, 10964-10967.

[38] N. Bontempi, E. Biavardi, D. Bordiga, G. Candiani, I. Alessandri, P. Bergese, E. Dalcanale, *Nanoscale* **2017**, *9*, 8639-8646.

[39] N. Kostlánová, E. P. Mitchell, H. Lortat-Jacob, S. Oscarson, M. Lahmann, N. Gilboa-Garber, G. Chambat, M. Wimmerová, A. Imberty, *J. Biol. Chem.* **2005**, *280*, 27839–27849.

[40] J. Arnaud, K. Tröndle, J. Claudinon, A. Audfray, A. Varrot, W. Römer, A. Imberty, *Angew. Chem. Int. Ed.* **2014**, *53*, 9267-9270.

[41] P. M. Antonik, A. N. Volkov, U. N. Broder, D. Lo Re, N. A. J. van Nuland, P. B. Crowley, *Biochemistry*, **2016**, *55*, 1195-1203.

[42] P. M. Antonik, A. M. Eissa, A. R. Round, N. R. Cameron, P. B. Crowley, *Biomacromol.* **2016**, *17*, 2719-2725.

[43] S. T. Larda, M. P. Bokoch, F. Evanics, R. S. Prosser, *J. Biomol. NMR.* **2012**, *54*, 199-209.

[44] S. Yi, A. E. Kaifer, *J. Org. Chem.* **2011**, *76*, 10275-10278.

[45] C. S. Beshara, C. E. Jones, K. D. Daze, B. J. Lilgert, F. Hof, *ChemBioChem* **2010**, *11*, 63-66.

[46] MeFuc binding was not perturbed by **Q7** binding, see Figure S8.

[47] S. Lim, H. Kim, N. Selvapalam, K. J. Kim, S. J. Cho, G. Seo, K. Kim, *Angew. Chem. Int. Ed.* **2008**, *47*, 3352-3355.

[48] D. Bardelang, K. Banaszak, H. Karoui, A. Rockenbauer, M. Waite, K. Udachin, J. A. Ripmeester, C. I. Ratcliffe, O. Ouari, P. Tordo, *J. Am. Chem. Soc.* **2009**, *131*, 5402-5404.

[49] D. Bardelang, K. A. Udachin, D. M. Leek, J. C. Margeson, G. Chan, C. I. Ratcliffe, J. A. Ripmeester, *Cryst. Growth Des.* **2011**, *11*, 5598-5614.

[50] Y.-M. Jeon, J. Kim, D. Whang, K. Kimoon, *J. Am. Chem. Soc.* **1996**, *118*, 9790-9791.

[51] B. Maity, S. Abe, T. Ueno, *Nat. Commun.* **2017**, *8*, 14820.

WILEY-VCH

COMMUNICATION

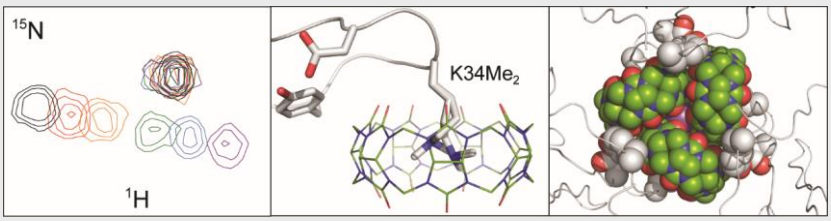

*Francesca Guagnini, Paweł M. Antonik, Martin L. Rennie, Peter O'Byrne, Amir R. Khan, Roberta Pinalli, Enrico Dalcanale, and Peter B. Crowley**

Page No. – Page No.

Cucurbit[7]uril–Dimethyllysine Recognition in a Model Protein

WILEY-VCH